Biochem. J. (2011) **436**, 71–81 (Printed in Great Britain) doi:10.1042/BJ20100884

online data

Identification and characterization of an inhibitory fibroblast growth factor receptor 2 (FGFR2) molecule, up-regulated in an Apert Syndrome mouse model

Lee M. WHELDON*[1], Naila KHODABUKUS*, Susannah J. PATEY*, Terence G. SMITH†, John K. HEATH* and Mohammad K. HAJIHOSSEINI†[2]

*School of Biosciences, University of Birmingham, Edgbaston B15 2TT, U.K., and †School of Biological Sciences, University of East Anglia, Norwich, Norfolk NR4 7TJ, U.K.

AS (Apert syndrome) is a congenital disease composed of skeletal, visceral and neural abnormalities, caused by dominant-acting mutations in FGFR2 [FGF (fibroblast growth factor) receptor 2]. Multiple FGFR2 splice variants are generated through alternative splicing, including PTC (premature termination codon)-containing transcripts that are normally eliminated via the NMD (nonsense-mediated decay) pathway. We have discovered that a soluble truncated FGFR2 molecule encoded by a PTC-containing transcript is up-regulated and persists in tissues of an AS mouse model. We have termed this IIIa–TM as it arises from aberrant splicing of FGFR2 exon 7 (IIIa) into exon 10 [TM (transmembrane domain)]. IIIa–TM is glycosylated and can modulate the binding of FGF1 to FGFR2 molecules in BIAcore-binding assays. We also show that IIIa–TM can negatively regulate FGF signalling *in vitro* and *in vivo*. AS phenotypes are thought to result from gain-of-FGFR2 signalling, but our findings suggest that IIIa–TM can contribute to these through a loss-of-FGFR2 function mechanism. Moreover, our findings raise the interesting possibility that FGFR2 signalling may be a regulator of the NMD pathway.

Key words: Apert syndrome, fibroblast growth factor receptor 2 (FGFR2), mRNA splicing, nonsense-mediated decay (NMD) pathway.

INTRODUCTION

Loss-of-function studies have demonstrated that FGF (fibroblast growth factor) signalling is a critical mediator of cellular interactions that underlie tissue development, repair and homoeostasis. For example, the growth of lungs and limbs is arrested in *Fgf10*-null embryos and adult *Fgf23*-deficient mice develop hyperphosphataemia [1,2]. However, subtle defects can also arise from partial-loss- or gain-of-FGF signalling, suggesting that the level of FGF signal perceived by target cells is also important [3–5]. This is exemplified by AS (Apert syndrome) and Pfeiffer syndrome, which are hallmarked by a host of skeletal, visceral and neural defects arising from dominant-acting mutations in FGFR1 (FGF receptor 1) and FGFR2 [6]. Therefore identifying the set of factors and mechanisms that regulate the dynamics of FGF signalling will further our understanding of growth factor signalling in developmental and disease processes.

The mammalian FGF signalling system comprises 18 FGF ligands and four transmembrane FGFRs (FGFR1–FGFR4), and can operate both in a morphogen and a threshold-dependent signalling manner [7–9]. Formation of a trimeric complex of FGFs, sulfated proteoglycans and membrane-anchored FGFR molecules results in the recruitment of intracellular adaptor proteins by the activated FGFRs and signal transduction to the nucleus via the MAPK (mitogen-activated protein kinase), PI3K (phosphoinositide 3-kinase) or PLC (phospholipase C) signalling pathways. Typically, FGF signalling induces changes in gene expression and/or cytoskeletal reorganization to regulate multiple aspects of cell behaviour and fate. The level and threshold of FGF signalling is modulated intracellularly through the activity of proteins such as Sprouty, MKP3 (MAPK phosphatase 3), Spred and Sef, and by the synergistic or antagonistic effects of other signalling pathways, including Notch, Wnts, BMPs (bone morphogenetic proteins), Hedgehogs etc. [5,10]. Extracellular regulation, by contrast, is dependent mostly on the bioavailability of FGFs and FGFRs, as well as factors that modulate their interactions such as FLRTs (fibronectin leucine-rich transmembrane proteins) and Klotho [11,12].

FGFR molecules are typically composed of two or three extracellular Ig-like domains (Ig-I, Ig-II and Ig-III) harbouring the ligand-binding sites, a single-pass TM (transmembrane) domain, an intracellular juxtamembrane domain, and a split tyrosine kinase domain. Alternative splicing of FGFR transcripts generates multiple receptor isoforms and contributes to the functional diversity of FGF signalling [7,13]. For example, the VT+ or VT− isoforms of FGFR1, which harbour or lack amino acids Val^{428} and Thr^{429} in the juxtamembrane domain respectively, engage different signalling pathways [14]. Moreover, the so-called 'IIIb' and 'IIIc' spliced isoforms of FGFR1–FGFR3 are formed through alternative usage of exons 8 and 9, which encode the C-terminal half of Ig-III [15], i.e. exon 7 (IIIa)–8 (IIIb)–10 (TM) or exon 7 (IIIa)–9 (IIIc)–10 (TM) splice variants. These isoforms

Abbreviations used: AS, Apert syndrome; BCIP, 5-bromo-4-chloroindol-3-yl phosphate; Dig, digoxygenin; DTT, dithiothreitol; E, embryonic day; ERK, extracellular-signal-regulated kinase; FGF, fibroblast growth factor; FGFR, FGF receptor; FL, fluorescence; GFP, green fluorescent protein; HEK-293T cells, human embryonic kidney-293 cells expressing the large T-antigen of simian virus 40; HRP, horseradish peroxidase; IEF, isoelectric focusing; Lamp2, lysosome-associated membrane protein 2; MAPK, mitogen-activated protein kinase; MKP3, MAPK phosphatase 3; NMD, nonsense-mediated decay; Nt, N-terminal; PNGase-F, peptide N-glycosidase F; PTC, premature termination codon; R_{max}, maximum analyte binding capacity; RT, reverse transcription; RU, response unit; R_{eq}, RUs corresponding to steady-state equilibrium; SPR, surface plasmon resonance; TM, transmembrane.

[1] Present address: Molecular Biology and Immunology Group, Centre for Biomolecular Sciences, University of Nottingham, Nottingham NG7 2RD, U.K.
[2] To whom correspondence should be addressed (email m.k.h@uea.ac.uk).

play critical roles in the paracrine cross-talk between epithelial and mesenchymal cells, since IIIb isoforms are predominant in the former and activated by mesenchymally produced FGF ligands (FGF3, FGF7, FGF10 and FGF22), whereas the IIIc receptor isoforms are expressed by mesenchymal (and neural) cells and are activated by a different set of FGFs (FGF2, FGF4, FGF8, FGF9 and FGF18) produced by epithelial cells [16].

Less clear is the biological significance of soluble FGFR isoforms. These include a molecule that specifically lacks the TM domain, or truncated receptors that harbour Ig-II and Ig-IIIa, with or without fusion to the first three amino acids of the TM domain or non-coding intronic sequences [7,17,18]. Some of these truncated receptors are encoded by PTC (premature termination codon)-containing transcripts [7], and are probably eliminated by the NMD (nonsense-mediated decay) pathway machinery [19].

Through gene targeting in ES (embryonic stem) cells, we have previously generated mice with an AS-type FGFR2 mutation [20]. In these, as in some patients, a heterozygous deletion of FGFR2 exon 9 (IIIc) (i.e. FgfR2-IIIc$^{+/\Delta}$) results in the aberrant co-expression of FGFR2-IIIb and FGFR2-IIIc isoforms in mesenchymal and neural cells [21,22]. Consequently, the affected tissues become promiscuously responsive to a broader set of FGF ligands and a gain-of-FGFR2 function ensues. We validated this mechanism by showing that much of the AS-like phenotypes in FgfR2-IIIc$^{+/\Delta}$ mice can be rescued merely by knocking down the levels of FGF10, a key FgfR2-IIIb-activating ligand [23].

We now report that FgfR2-IIIc$^{+/\Delta}$ tissues additionally harbour a PTC-derived truncated FGFR2 molecule that we term 'IIIa–TM'. IIIa–TM arises from direct splicing of exon 7 (IIIa) into 10 (TM) to encode a molecule that harbours the Ig-I, Ig-II and the N-terminal half of Ig-III (IIIa) domains fused to the first three amino-acids of TM. We have explored the biochemical properties of IIIa–TM and find that it has some ligand-binding capacity. Moreover, IIIa–TM is capable of attenuating basal FGFR signalling *in vitro* and *in vivo*, and influences the trafficking of endogenous FGFR2 molecules. Our findings suggest that IIIa–TM escapes NMD and acts as a negative regulator of FGFR signalling to cause or contribute to the severity of phenotypes in AS, which were otherwise thought to arise solely through gain-of-FGFR2 activity.

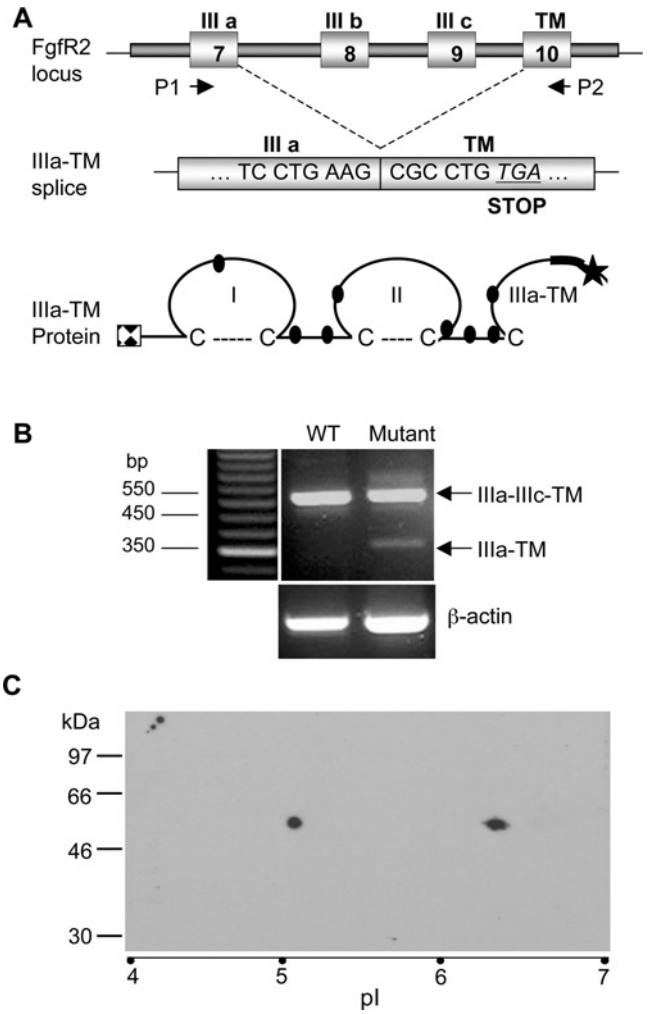

Figure 1 Structure and detection of IIIa–TM in FgfR2-IIIc$^{+/\Delta}$ (mutant) mice

(**A**) Schematic representation of the *FgfR2* locus and the aberrant splicing of exon 7 (IIIa) into 10 (TM) which yields a PTC-containing transcript and a truncated protein with eight potential glycosylation sites (black circles). Chequered box, secretory signal sequence; bold line, contribution of TM exon; star, termination codon. (**B**, **C**). Detection of IIIa–TM transcript and protein in the mutant but not wild-type (WT) brain. (**B**) The use of Primers P1 and P2 (positions indicated in **A**) in RT–PCRs generated two products from mutant RNA. Note, neural tissue expresses the IIIc isoform of FGFR2 [24]. (**C**) The detergent-soluble fractions of mutant brain tissue resolved on two-dimensional gels and immunoprobed with anti-FGFR2 antibodies. Two major 55 kDa products (pIs 5.1 and 6.3) and a minor 120 kDa (pI 4.3) product are evident. No spots were detected in blots of wild-type tissue.

MATERIALS AND METHODS

Animals and tissue source

FgfR2-IIIc$^{floxed/+}$ and PGK (phosphoglycerol kinase)-Cre mice were used to derive the FgfR2-IIIc$^{+/\Delta}$ mutant mice/tissues, as described previously [20,23]. All mice were bred and maintained on C57BL background in accordance with Home Office licences and local regulations governing animal welfare and ethics.

Detection, isolation and cloning of IIIa–TM

RNA was isolated from brains of newborn wild-type or FgfR2-IIIc$^{+/\Delta}$ (mutant) mice using Tri reagent (Sigma), and subjected to two-step RT (reverse transcription)–PCRs using Ready-to-Go beads (Amersham Pharmacia) and cycle conditions described previously [20,24]. The IIIa–TM transcript (Figure 1A) was detected using Primers P1 (5′-CCCATCCTCCAAGCTGGACTGCCT-3′) and P2 (5′-GCTTGGTCAGCTTGTGCACAGCTGG-3′). 'Full-length' FGFR2-IIIa–TM was amplified using an NdeI-tagged primer P3 (5′-AGTTTAGTTGAGGATACCACTTTAG-3′) in conjunction with an NotI-tagged primer P4 (5′-TCACAGGCGCTTCAGGACCTTG-3′). Products were sequenced using forward or reverse complements of primers P1 and P5 (5′-CGTGATCAGTTGGACTAAGGATGG-3′; nucleotides 815–835 of *FgfR2*; GenBank® accession number, NM_010207) (see Supplementary Figure S1 at http://www.BiochemJ.org/bj/436/bj4360071add.htm). A 0.9 kb recombinant IIIa–TM was generated by primers P2 and P3, gel-purified and cloned into a 7.9 kb ires-Topaz-pEF-BOS plasmid, downstream of sequences encoding the human FGFR2 secretory signal sequence, IgG-Fc and a 3C-protease-sensitive site (see Supplementary Figure S2 at http://www.BiochemJ.org/bj/436/bj4360071add.htm). To examine the distribution of native IIIa–TM protein, lungs or brains of wild-type and mutant newborn mice were triturated through a 19G gauge needle and protein was extracted by incubation for 30 min at 4 °C in 500 μl of RIPA buffer (10 mM Tris/HCl, pH 7.4,

1 mM EGTA, 150 mM NaCl, 0.1% SDS, 1% Nonidet P40, 0.5% sodium deoxycholate, 1 mM PMSF and 1 mM Na_3VO_4) containing protease inhibitor cocktail (Roche). Tissue lysates were cleared by centrifugation (20800 ***g*** for 60 min at 4 °C) and protein concentrations were determined by Coomassie assay (Pierce).

Maintenance and transfection of cell lines

HEK-293T cells (human embryonic kidney-293 cells expressing the large T-antigen of simian virus 40) and Cos7 cells were maintained at 37 °C in a humidified atmosphere of 5% CO_2 in DMEM (Dulbecco's modified Eagle's medium), supplemented with 10% FBS (fetal bovine serum), 2 mM L-glutamine, 1 mM sodium pyruvate, 0.2 unit/ml penicillin and 0.1 mg/ml streptomycin. Plates containing HEK-293T cells at 70% confluency were transiently transfected using the calcium phosphate precipitation method overnight with plasmid DNA (30, 60 or 300 μg) diluted in 2 M $CaCl_2$ and 2× HBS (1.2% Hepes, 1.6% NaCl and 0.04% Na_2HPO_4, pH 7.12). Cells were then washed with serum-free medium and maintained in the same medium or Ultracho medium (Biowhittaker).

Antibodies

The primary antibodies used were: sheep anti-FGFR2(Nt) (N-terminal) (1:2000–10000 dilution; [25]), rabbit anti-Bek (cytoplasmic FGFR2, 1:500–1000 dilution; C-17, Santa Cruz Biotechnology), mouse anti-ERK (extracellular-signal-regulated kinase) and anti-phospho-ERK (1:1000 and 1:2000 dilution respectively; Cell Signaling Technology), mouse anti-Lamp2 (lysosome-associated membrane protein 2) (1:50 dilution; Abcam), and HRP (horseradish peroxidase)-conjugated goat anti-(human Fc) (1:10000 dilution; Pierce). The secondary antibodies used were HRP-conjugated anti-(mouse Ig), anti-(rabbit Ig) (1:5000 dilution; Amersham Biosciences) and anti-(sheep Ig) (1:4000 dilution; The Binding Site), FITC-conjugated anti-(rabbit Ig) (1:300 dilution) and Texas Red-conjugated anti-(mouse Ig) (1:200 dilution; Molecular Probes).

Immunodetection and quantification of FGFR2 and Lamp2 co-localization

Cos7 cells were grown on glass coverslips and transfected with FGFR2 using Genejuice (Invitrogen). At 48 h later, cells were fixed with 4% paraformaldehyde (10 min), permeabilized with ice-cold methanol and re-hydrated in PBS. After incubation for 1 h in PBS/4% BSA, the cells were exposed to anti-Lamp2 and anti-Bek antibodies for 1 h. Coverslips were then washed in PBS and incubated with the relevant secondary antibodies for 1 h, washed in PBS/0.1% Tween 20 and mounted using Mowiol medium. Images of immunolabelled cells were captured using a confocal microscope (Leica), processed in Adobe Photoshop and merged using ImageJ. To quantify the co-localization of FGFR2 and Lamp2, 15 random images from different treatments across two different experiments were analysed and a co-efficient was determined using ZEN 2009 software. Mean (±S.E.M.) values were subjected to analysis using a Student's *t* test. A one-way ANOVA indicated no variance with respect to time of FGF2 stimulation in the absence of IIIa–TM (see Figure 5A for paradigm), but a significant difference in its presence ($*P < 0.05$ and $***P < 0.0001$). Dunnett's Multiple comparison test also confirmed a significant abrogation of FGFR2/Lamp2 co-localization in the presence of IIIa–TM-only.

Immunoprecipitation of FGFR2

Protein was extracted from pellets of transiently transfected HEK-293T cells by incubation for 30 min in a lysis buffer (10 mM Tris/HCl, pH 8, 2.5 mM $MgCl_2$, 5 mM EGTA, 0.5% Triton X-100, 1 mM Na_3VO_4 and 50 mM sodium fluoride) containing protease inhibitor cocktail (Roche). After removing cell debris, the Triton X-100-insoluble fraction was isolated by centrifugation, and FGFR2 was immunoprecipitated from the supernatant with 3.5 μg of anti-Bek antibodies for 1 h at 4 °C. Immunocomplexes were captured with a 50% Protein A–Sepharose slurry for 30 min at 4 °C, and samples were washed twice with ice-cold hcTBST (100 mM Tris/HCl, 1.5 M NaCl and 0.05% Tween 20, pH 7.4), followed by ice-cold TE buffer (10 mM Tris/HCl and 1 mM EDTA, pH 7.5). The resultant samples were boiled for 5 min and subjected to SDS/PAGE and immunoblotting analyses.

SDS/PAGE and protein detection

Proteins were separated by SDS/PAGE and transferred on to nitrocellulose membranes (Protran BA85; Schleicher & Schuell) using a Biometra semi-dry transfer system at 5 mA/cm^2 of gel for 25 min. Membranes were blocked overnight at 4 °C with TBST (20 mM Tris/HCl, 140 mM NaCl and 0.1% Tween 20, pH 7.4) containing 5% BSA and then incubated for 1 h at room temperature (22 °C) with the relevant primary antibodies. Secondary antibodies were applied for 1 h at room temperature and, following washes in TBST, immunoreactive bands were detected with ECL (enhanced chemiluminescence) reagents (Pierce). Where necessary, membranes were stripped in 0.1 M glycine (pH 2.5), washed sequentially in TBST and TBST/5% BSA and re-probed overnight at 4 °C.

Purification of Fc-tagged proteins

3CFc, IIIa–TM–3CFc, FGFR2-IIIb–3CFc and FGFR2-IIIc–3CFc proteins were harvested from HEK-293T cells or their conditioned medium 24 h (48 h for IIIa–TM) after transfection with the relevant plasmids [25]. 3CFc-tagged proteins were purified by gravity flow over a Protein A–Sepharose fast-flow column equilibrated previously with MT-PBS (150 mM NaCl, 16 mM Na_2HPO_4 and 4 mM NaH_2PO_4, pH 7.4). Columns were then washed successively with MT-PBS/1% Triton X-100, MT-PBS alone and finally 50 mM Tris/HCl (pH 8) and 150 mM NaCl solution. Proteins were eluted from the column with 0.1 M glycine, pH 3, and dialysed overnight at 4 °C. To obtain cleaved recombinant IIIa–TM, the column was washed with TNED [50 mM Tris/HCl, pH 8, 150 mM NaCl, 10 mM EDTA and 1 mM DTT (dithiothreitol)] and treated overnight at 4 °C with 10 μg of 3C protease. Cleaved IIIa–TM was then dialysed into PBS.

PNGase-F (peptide N-glycosidase F) treatment

Purified IIIa–TM protein (1 mg) was boiled for 10 min in a solution containing 50 mM Tris/HCl, pH 8, 150 mM NaCl, 10 mM EDTA, 1 mM DTT, 0.5% SDS and 1% 2-mercaptoethanol, and treated for 16 h at 37 °C with 5 units of PNGase-F (New England Biolabs) in a solution of 50 mM Na_2HPO_4 (pH 7.5) and 1% Nonidet P40.

Two-dimensional gel electrophoresis

A portion (100 mg) of tissue-extracted protein or 900 ng of recombinant IIIa–TM protein was mixed with 125 μl of

rehydration buffer (8 M urea, 2 % CHAPS, 20 mM DTT, 0.5 % IPG buffer and a trace of Bromophenol Blue) and loaded into a strip holder. An IPG drystrip (7 cm, pH 4–7 immobilized linear gradient; Amersham Pharmacia) was overlaid on to the rehydration buffer containing the sample and rehydrated overnight at 20 °C. Optimal IEF (isoelectric focusing) was carried out using an IPGphor step-n-hold and the following protocol: 500 V for 500 Vh, 1000 V for 1000 Vh and 8000 V for 16000 Vh, all at 20 °C. Strips were then immediately processed for SDS/PAGE or stored at − 70 °C until required.

For SDS/PAGE, IEF strips were equilibrated for 20 min at a time with equilibration buffer 1 (50 mM Tris/HCl, pH 8.8, 6 M urea, 30 % glycerol, 2 % SDS, 60 mM DTT and a trace of Bromophenol Blue), followed by equilibration buffer 2 (same as buffer 1, but DTT was replaced with 25 mg/ml iodoacetamide). Drystrips were sealed into wells (0.5 % agarose in running buffer) and samples were then resolved on vertical gels by SDS/PAGE at 110 V for 10 min, followed by 200 V for 30 min. Protein spots were visualized by chemiluminescence after transfer to nitrocellulose, as described above.

SPR (surface plasmon resonance) analysis

All protein interactions were measured using a BIAcore 2000. 3CFc-tagged proteins were immobilized in 10 mM sodium acetate, pH 4.5, on to a research-grade C1 sensor chip (BIAcore), according to the manufacturer's instructions, at a flow rate of 10 μl/min. Proteins were immobilized to similar levels [$\sim$1000 RUs (response units) above the pre-injection baseline; $\sim$400 RUs for 3CFc owing to a difference in molecular mass] and the excess carboxy groups were then blocked by an injection of 70 μl of 1 M ethanolamine, pH 8.5. Binding experiments were performed in HBS-EP (0.01 M Hepes, pH 7.4, 0.15 M NaCl, 3 mM EDTA and 0.005 % surfactant P-20) (BIAcore) at a flow rate of 50 μl/min using various concentrations of FGF1 ligand (J.K.H. Laboratory) and IIIa–TM proteins diluted in HBS-EP. Residual bound FGF and IIIa–TM were removed with injections of 2 M NaCl and 10 mM HCl. Reference responses from 3CFc flow cells were subtracted for each analyte concentration using BiaEvaluation software (BIAcore). Disturbances at the start and end of the sensorgrams were excluded from curve fitting analysis. Kinetic and R_{eq} (RUs coresponding to steady-state equilibrium) data were derived using four different analyte concentrations and a Langmuir model of binding (1:1) for curve fitting. Following curve fitting, each sensorgram was manually examined for the closeness of the fit. χ^2 was <10 % of R_{max} (R_{max}, maximum analyte binding capacity) in all cases.

Chick embryo manipulations and *in situ* hybridization

The somites of Hamburger and Hamilton stage 17–21 chick embryos were electroporated with 2 mg/ml of purified plasmids encoding IIIa–TM or GFP (green fluorescent protein; as control) using a protocol described previously [26]. After incubation for 5–7 h of at 37 °C, electroporated embryos were fixed in 4 % PFA (paraformaldehyde) and processed for *in situ* hybridization using Dig (digoxygenin)- or FL (fluorescence)-tagged antisense *Mkp3* or GFP riboprobes. The *in situ* signal was detected using AP (alkaline phosphatase)-tagged anti-Dig and anti-FL antibodies [26]. GFP was visualized in orange by using an INT (2-*p*-iodophenyl-3-*p*-nitrophenyl-5-phenyltetrazolium chloride)/BCIP (5-bromo-4-chloroindol-3-yl phosphate) solution, whereas Mkp3 was visualized in purple with NBT (Nitro Blue Tetrazolium)/BCIP solutions (Roche; see Figure 5C). Use of control sense labels did not yield any signal.

RESULTS

Widespread expression and persistence of IIIa–TM in FgfR2-IIIc$^{+/\Delta}$ tissues

Splicing of FGFR2 exon 7 (IIIa) into 10 (TM) should yield a 317 amino-acid-long soluble FGFR2 molecule (IIIa–TM; Figure 1A) with a predicted molecular mass of 35.5 kDa (if non-glycosylated) and pI of 5.88. In order to contribute to FgfR2-IIIc$^{+/\Delta}$ (subsequently referred to as 'mutant') phenotypes, IIIa–TM should survive NMD and be detectable at both the transcript and protein levels.

Using standard RT–PCRs and primers specific to exons 7 (IIIa) and 10 (TM) respectively, we detected low levels of IIIa–TM spliced transcripts in RNA derived from the brains of mutant but not wild-type mice (Figure 1B). To examine whether IIIa–TM was present as a 'full-length' FGFR2 molecule, we used primers from FGFR2 exon 2 and the IIIa–TM splice junction, and successfully amplified an 873 bp 'full-length' transcript. DNA sequencing confirmed that this product encodes Ig-I, the 'acid-box', Ig-II and Ig-IIIa, spliced to the first nine bases of exon 10 (Supplementary Figure S1). IIIa–TM transcripts were found in diverse tissues and all stages examined, namely in the mutant embryonic forebrain [E (embryonic day) 14.5], hindbrain (E9.5), lungs (E14.5) and newborn lung, liver and kidneys, but never in comparable wild-type siblings (results not shown).

To examine whether the IIIa–TM transcripts are translated into protein *in vivo*, we subjected the soluble fraction of protein isolated from wild-type and mutant tissues to two-dimensional gel analysis over a pI range of 4–7, and probed the resulting blots with antibodies that only detect the ectodomain of FGFR2 [the anti-FGFR2(Nt) antibody]. Two major immunoreactive spots of apparent molecular mass of 55 kDa (pI 5.1 and 6.3) and a minor 120 kDa spot (pI 4.3) were detectable in the mutant (Figure. 1C), but not wild-type samples. Equal loading of protein in these assays was confirmed by anti-tubulin labelling (results not shown).

Taken together, these findings demonstrate that IIIa–TM is present and could modulate FGF signalling in the mutant tissues.

Biochemical characterization of recombinant IIIa–TM protein

To explore the biochemical and binding properties of IIIa–TM, we generated a recombinant protein. Using RT–PCR, we first amplified a 0.87 kb IIIa–TM cDNA fragment lacking the endogenous FGFR2 signal sequence, and cloned this into an ires-Topaz-pEF-BOS plasmid, downstream of sequences composed of human FGFR2 secretory signal sequence, human IgG-Fc and a 3C-protease-sensitive site (Figure 2A and Supplementary Figure S2). The resulting recombinant protein (subsequently termed IIIa–TM–3CFc) was isolated from the supernatant of transiently transfected HEK-293T cells using Protein A–Sepharose (Figure 2B). The recombinant IIIa–TM protein was produced optimally at 60 h post-transfection, but thereafter it was down-regulated or degraded (results not shown).

To further characterize soluble IIIa–TM, the Fc domain of recombinant IIIa–TM–3CFc was cleaved by 3C protease digestion. We found that in solution the 3C-cleaved IIIa–TM protein formed multiple higher molecular-mass products (e.g. 110 kDa) (Figure 2C), which, in the presence of the reducing agent DTT (200 mM), were reduced to a multiple immunoreactive species of approximately 55 kDa (Figure 2C, lane 2). Probably, these higher-order products result from dimeric or oligomeric association of the native $\sim$55 kDa protein, via disulfide bonding

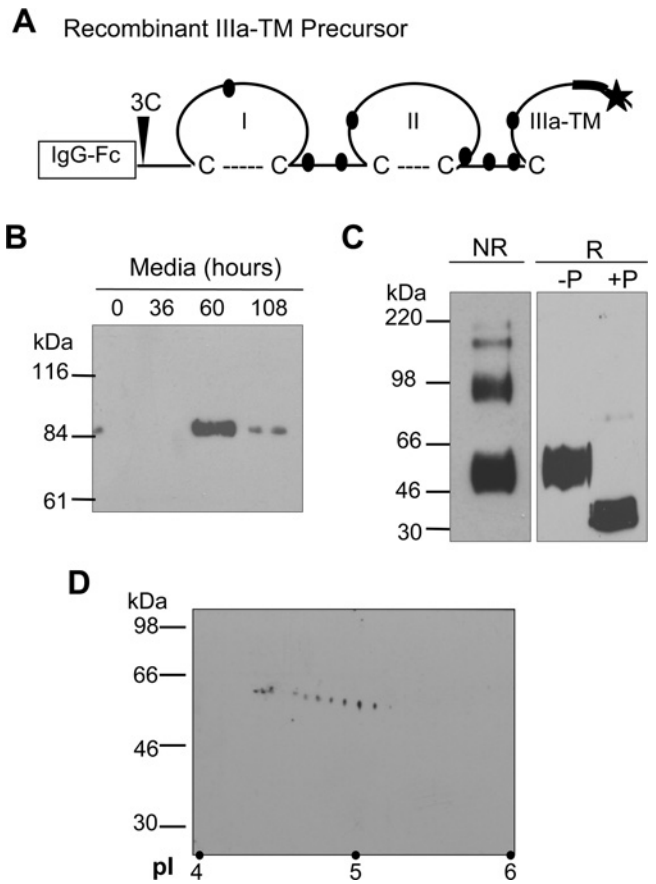

Figure 2 Generation and biochemical characterization of recombinant IIIa–TM protein

(**A**) The recombinant IIIa–TM protein was fused to the IgG-Fc domain to aid in the purification process and carries a 3C-protease-sensitive site (arrow head) to allow cleavage of the IgG-Fc domain. (**B**) Recombinant 3CFc–IIIa–TM was optimally detected in the supernatant of HEK-293T cells at 60 h post-transfection. (**C**) SDS/PAGE analysis of purified IIIa–TM protein revealed distinct oligomeric complexes of 55–200 kDa under non-reducing conditions (NR). Under reducing conditions (R), a single ~50 kDa product was detected, which was reduced further to ~35 kDa after deglycosylation by PNGase-F treatment (R + P; lane 3). (**D**) Two-dimensional gel analysis over the pI range 4–7 revealed that HEK-293T-cell-expressed IIIa–TM can exist in multiple glycosylated forms in the range of 55–60 kDa.

of the unpaired cysteine residue present on the IgIII domain of IIIa–TM (Figure 2A), as observed in soluble FGFR1 and FGFR3 molecules [17,27].

IIIa–TM contains eight putative N-glycosylation sites (Figure 1A and Supplementary Figure S1), a subset of which must be glycosylated if IIIa–TM, like other FGFRs, is to interact with FGF ligands. To test this, we removed the N-linked oligosaccharide residues from 3C-cleaved IIIa–TM by PNGase-F treatment and found that the apparent mass of the native protein was reduced from 55 to 35 kDa (Figure 2C, lane 3). Moreover, resolution of HEK-293T cell-derived recombinant IIIa–TM on two-dimensional gels yielded eight distinct products of different molecular masses and pIs (Figure 2D), suggesting that these are multiple order glycoforms. These findings can explain why IIIa–TM appears as a broad band on a standard SDS/PAGE gel (Figure 2C, lane 2) and also raise the possibility that the two spots observed in Figure 1(C) represent two different glycoforms of IIIa–TM in the mutant brain *in vivo*.

IIIa–TM can modulate the binding kinetics of FGF1 to FGFR2 molecules

As a secreted truncated receptor, IIIa–TM could interfere with FGFR2 signalling either by sequestering FGF ligands away from FGFRs and/or forming non-functional heterodimers with full-length FGFRs themselves. However, both of these processes require an interaction between FGF ligand(s) and IIIa–TM. We therefore used the well-characterized BIAcore assay [28] to investigate the dynamics of such interactions, either in the presence or absence of recombinant FGFR2-IIIb or FGFR2-IIIc ectodomain molecules.

First, a series of Fc-tagged proteins were generated in HEK-293T cells by transfection with plasmids encoding IIIa–TM–3CFc, FGFR2-IIIb–3CFc, FGFR2-IIIc–3CFc or 3CFc as control. Purified proteins were immobilized on to a BIAcore C1 sensor chip in equimolar amounts and then different concentrations of FGF1 were perfused across the sensor chip in the absence of heparin in order to examine receptor–ligand interactions. FGF1 was chosen because it interacts with all FGFRs/FGFR isoforms [16]. BIAcore assays measure the rate of association followed by dissociation of free and chip-anchored proteins. To evaluate these parameters, we obtained the plasmon resonance values and normalized them against values obtained by binding of FGF1 to the control protein 3CFc.

As shown in Figure 3 and Table 1, FGF1 bound chip-anchored FGFR2-IIIb and FGFR2-IIIc molecules with similar affinity ($K_d = 5.14 \times 10^{-10}$ and 7.05×10^{-10} respectively), but showed no discernible binding to chip-anchored IIIa–TM (Figure 3D). The latter observation is probably explained by the absence of the C-terminal half of the Ig-III-like domain from IIIa–TM [29].

In the presence of excess free IIIa–TM (i.e. 62.5 nM), however, FGF1 interacted with chip-anchored IIIa–TM ($K_d = 6.8 \times 10^{-8}$). Free IIIa–TM also caused more total protein interaction with chip-anchored FGFR2-IIIb and FGFR2-IIIc (Figures 3G–3I), but simultaneously reduced the binding affinity of FGF1 to chip-anchored FGFR2-IIIb and FGFR2-IIIc by 5- and 10-fold respectively (Table 1). Importantly, we found that, in the absence of FGF1, excess free IIIa–TM did not bind to chip-anchored IIIa–TM, FGFR2-IIIb or FGFR2-IIIc (Figures 3A–3C).

Taken together, these findings demonstrate that, as a complex, IIIa–TM is capable of interacting with FGF1 and modulating its interactions with receptor molecules that contain the entire ligand-binding domain. By inference, IIIa–TM may attenuate FGF signalling through two mutually non-exclusive mechanisms: sequestering FGF ligands and/or forming non-functional heterodimers with FGFRs.

Exogenous IIIa–TM modulates the levels of FGFR signalling and trafficking of FGFR2

We next examined whether IIIa–TM alters the dynamics of FGFR signalling in cultured cells. Cos7 cells, which endogenously express the IIIc of FGFR1, FGFR2 and FGFR4 (Figure 4A) and FGF4 and FGF9 (M.K. Hajihossenini and L.M. Wheldon, unpublished work), were grown to confluency and serum-starved before being co-stimulated with FGF2 (20 ng/ml) and heparin (10 μg/ml), in the presence or absence of exogenously added 3C-cleaved IIIa–TM (5 μg/ml). Immunoblotting of total cell lysates with anti-ERK and phospho-ERK antibodies showed that the presence of IIIa–TM reduced the level of FGF signalling (Figure 4B). Immunoprecipitation of FGFR2 with antibodies against the cytoplasmic domain of FGFR2 (Bek; C17), followed by immunoblotting with anti-FGFR2(Nt) or anti-phosphotyrosine (phospho-Tyr^{20}/4G10 cocktail) antibodies,

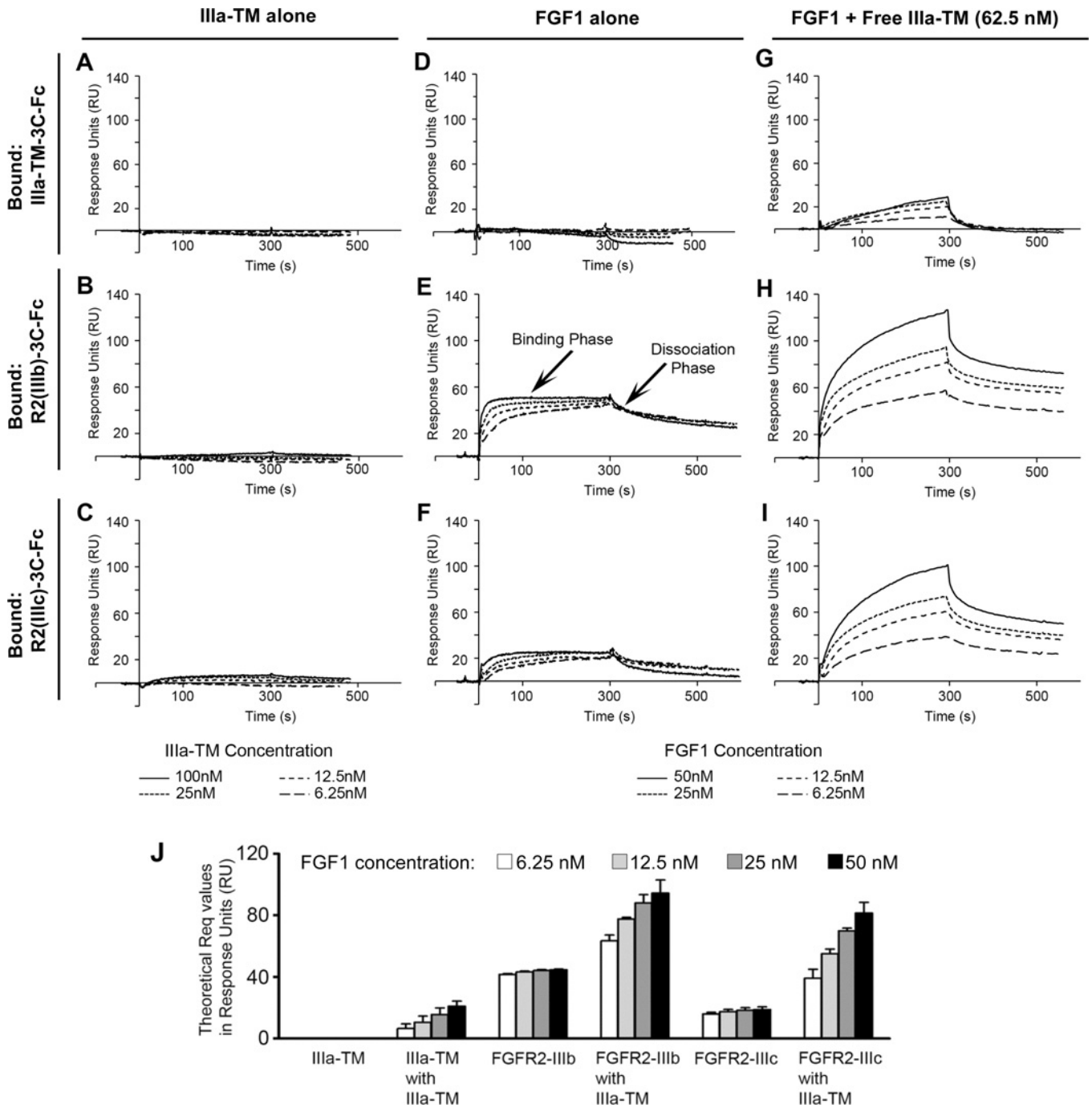

Figure 3 Binding kinetics of recombinant IIIa–TM to FGF1

Sensograms depicting the SPR analysis of FGF1 binding to immobilized 3CFc–IIIa–TM, 3CFc–FGFR2-IIIb and 3CFc–FGFR2-IIIc ectodomains in the absence (**D**–**F**) or presence (**G**–**I**) of free IIIa–TM. (**A**–**C**) Negligible binding of IIIa–TM alone to these ectodomains was observed. Boxes indicate the concentrations of IIIa–TM and FGF1 applied in each setting. Higher RUs (vertical axis) observed in (**G**–**I**), in the presence of excess IIIa–TM (62.5 nM), indicated that there was a net increase in interaction of FGF1 with the immobilized FGFR molecules. The corresponding kinetic data are summarized in Table 1. (**J**) Determination of theoretical R_{eq} values for FGF1–FGFR2 binding using four different analyte concentrations (boxes, 6.25–50 nM) and a Langmuir (1:1) model of binding for curve fitting. Values are means±S.E.M. of duplicates on the same chip and represent results from three separate chips.

revealed a clear inhibition of FGFR phosphorylation levels in the presence of IIIa–TM (Figure 4C).

Interestingly, we observed a decrease in levels of full-length FGFR2 in cells exposed to IIIa–TM and FGF2 combined (Figure 4C). This could be explained either by rapid destruction of FGFRs or, more likely, the translocation of FGFRs into a cellular compartment that is detergent-insoluble or inaccessible to the immunoprecipitating antibodies. Nonetheless, these changes demonstrate that exogenously added IIIa–TM can modulate FGFR2-mediated signalling levels in cultured cells.

To investigate how IIIa–TM has an impact on the trafficking of FGFR2 in cells, we transfected HEK-293T or Cos7 cells, which have low levels of endogenous FGFR2, with full-length FGFR2-encoding plasmids before treatment with exogenous

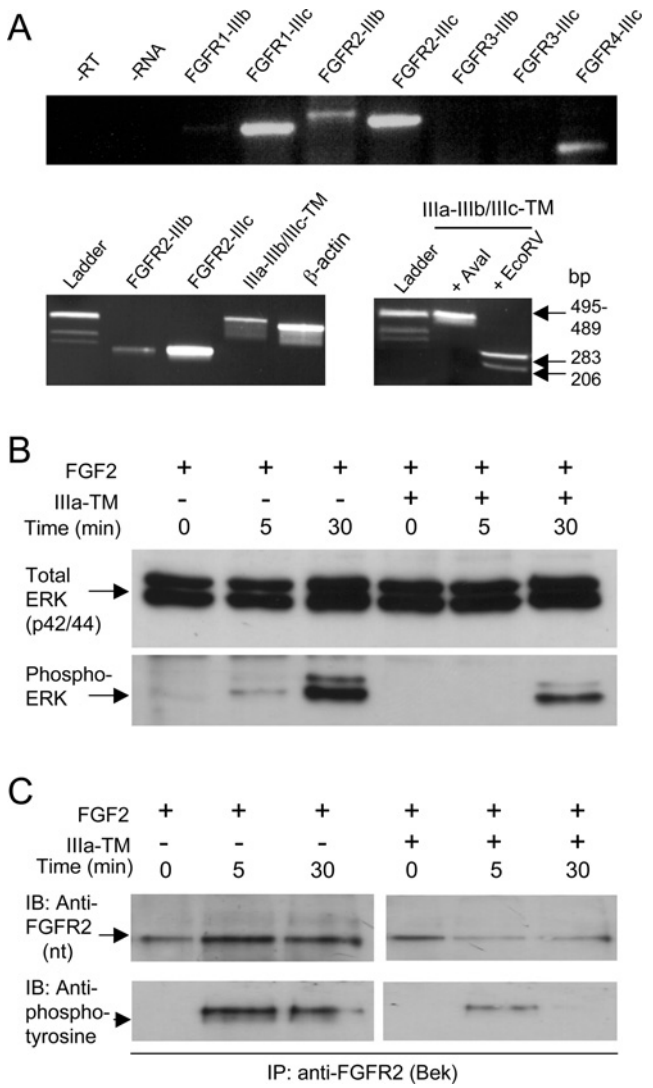

Figure 4 Exogenous IIIa–TM modulates the dynamics of FGFR signalling in HEK-293T cells

(**A**, upper panel) RT–PCR analysis using isoform-specific primers [20] showing that IIIc isoforms of FGFR1 and FGFR2 predominate in HEK-293T cells. This was confirmed further for FGFR2 (lower panel) as RT–PCR-amplified IIIa–IIIb–TM and IIIa–IIIc–TM products using common primers from FGFR2 IIIa and TM exons were digested by the EcoRV, but not the AvaI, enzyme [34]. (**B**) Stimulation of HEK-293T cells with the cognate ligand (FGF2) induced a time-dependent ERK activation in control cells (lower panel, lanes 1–3), which was attenuated by exogenous IIIa–TM (lower panel, lanes 4–6). Results are representative of three independent experiments. (**C**) Analysis of immunoprecipitated FGFR2 shows a marked reduction in the level of receptor tyrosine phosphorylation in the presence of IIIa–TM after both 5 and 30 min of FGF2 stimulation. IP, immunoprecipitation; IB, immunoblotting.

IIIa–TM in the presence or absence of FGF2 (Figure 5A). Co-immunolabelling of cells with anti-FGFR2(Nt) and anti-Lamp2 antibodies and quantification of their co-localization showed that, in the absence of IIIa–TM, significant levels of transfected FGFR2 was internalized into Lamp2-positive late endosomes and lysosomes, even when cells were treated with FGF2. In the presence of IIIa–TM, however, FGFR2 molecules appeared to accumulate at the cell membrane, more so when FGF2 was present, and showed reduced association with endosomes/lysosomes (Figures 5B–5H). These findings concur with the BIAcore data and suggest that IIIa–TM forms a complex with FGF ligands and receptors, which, in living cells, traps the receptors at the cell surface.

IIIa–TM can attenuate FGF signalling *in vivo*

Next, we tested whether IIIa–TM can also modulate FGFR signalling *in vivo* in chick embryos. We took advantage of previous findings that proper generation of chick somites (precursors to axial muscles) relies on FGFR signalling [26], such that electroporation of a dominant-negative (membrane-bound) FGFR construct or the application of the FGFR inhibitor SU5406 can disrupt normal somitogenesis. Attenuation of FGF signalling in this system is measured by the loss of *Mkp3* expression, which is a cytoplasmic modulator and a target of FGFR signalling itself [10,26].

Plasmids encoding IIIa–TM (2 μg/ml) or GFP were electroporated into the developing chick somites and *in situ* hybridization was used to detect GFP or *Mkp3* in the manipulated embryos ($n = 2$ of each treatment). As shown in Figure 6, introduction of IIIa–TM- but not GFP-encoding plasmids resulted in the loss of *Mkp3* expression, which is reminiscent of the attenuation of FGFR signalling by SU5402 or dominant-negative FGFRs [26]. These findings demonstrate that IIIa–TM interferes with FGFR signalling in an *in vivo* setting.

DISCUSSION

In the present study we show that a soluble FGFR2 molecule is up-regulated in FgfR2-IIIc$^{+/\Delta}$ mice, which model AS. We termed this molecule IIIa–TM, as it arises from aberrant splicing of FGFR2 exon 7 (IIIa) into exon 10 (TM). Neither the transcript nor IIIa–TM protein were detected in wild-type tissues/cells. Recombinant IIIa–TM generated in HEK-293T cells was found to be N-glycosylated and formed oligomeric complexes in solution. Using BIAcore sensor chip assays we found that IIIa–TM protein displays limited FGF ligand binding. Exogenous addition of IIIa–TM in the presence of FGF ligands efficiently attenuated FGFR signalling and interfered with receptor trafficking in cultured cells. Finally, introduction of IIIa–TM into the developing chick embryos attenuated FGFR signalling. Taken together, these findings suggest that IIIa–TM is in a position to induce loss-of-FGFR signalling in FgfR2-IIIc$^{+/\Delta}$ mice and, by inference, in AS.

FGFR2 is encoded by 19 exons that can generate a spectrum of alternatively spliced transcripts [7]. IIIa–TM is one such candidate, but it was not detected in normal cells either by RT–PCR (the present study) or RNAse protection assays [30]. This suggests that either splicing of exon 7 into 10 is a rare event or, more likely, that, as a PTC-containing transcript, IIIa–TM is normally destroyed by components of the NMD pathway. In general, the NMD machinery eliminates transcripts that carry a PTC positioned greater than 50–55 bp upstream of the last coding splice junction of a gene (for reviews, see [19,31]).

Interestingly, NMD is thought to play a critical role in regulating the expression levels of alternatively spliced genes, whereby the amount of useful transcripts destined for translation is titrated through active production and destruction of related PTC-harbouring transcripts [32,33]. Therefore IIIa–TM transcripts could play important role(s) in regulating the normal level of FGFR2 expression and signalling. However, when such transcripts persist, as in disease situations, they could assume entirely different regulatory roles.

It is not clear how and why IIIa–TM escapes NMD in FgfR2-IIIc$^{+/\Delta}$ tissues, but it is not a peculiarity of this allele as it can be

Table 1 Summary of kinetic data for FGF1 binding in the absence or presence of a 10-fold excess of soluble IIIa–TM

K_{on} and K_{off} were derived as described in the Materials and methods section. χ^2 was <10 % of R_{max} in all cases. The apparent affinity, K_d, is equal to K_{off}/K_{on}. NDB, no discernable binding.

		Analyte bound to C1 sensor chip (value by receptor isotype)		
Soluble analyte	Parameter	IIIa–TM–Fc	FGFR2-IIIb–Fc	FGFR-2IIIc–Fc
FGF1	K_{on} ($M^{-1} \cdot s^{-1}$)	NDB	3.93×10^{6}	2.41×10^{6}
	K_{off} (s^{-1})	NDB	2.02×10^{-3}	1.70×10^{-3}
	K_d (M)	NDB	5.14×10^{-10}	7.05×10^{-10}
FGF1 + IIIa–TM	K_{on} ($M^{-1} \cdot s^{-1}$)	1.77×10^{5}	3.48×10^{5}	2.75×10^{5}
	K_{off} (s^{-1})	1.20×10^{-2}	1.00×10^{-3}	2.00×10^{-3}
	K_d (M)	6.80×10^{-8}	2.87×10^{-9}	7.27×10^{-9}

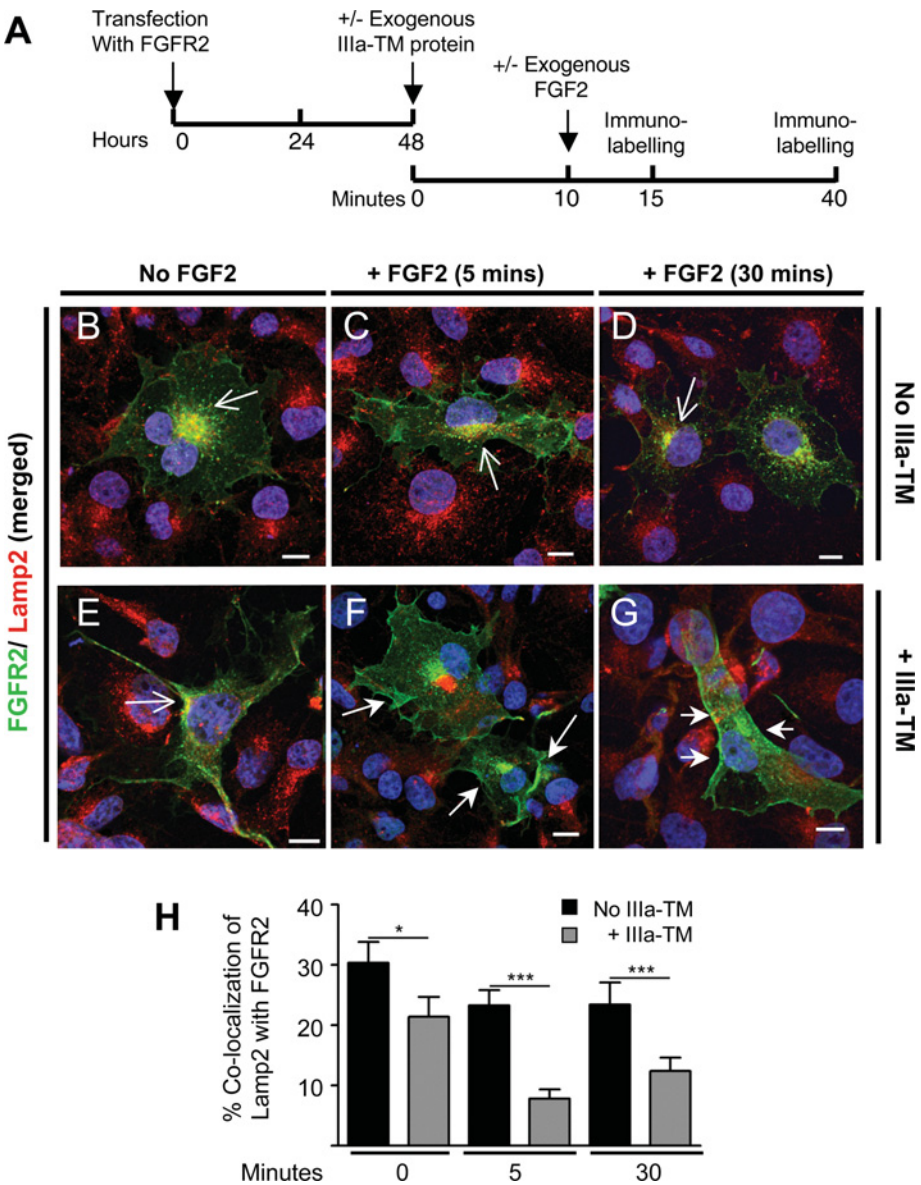

Figure 5 Exogenous IIIa–TM interferes with trafficking of FGFR2

(**A**) Experimental paradigm and time-course of analysis. (**B**–**G**) Differential localization of FGFR2 in transfected Cos7 cells after their stimulation with exogenous FGF2 (20 ng/ml), heparin (10 μg/ml) and IIIa–TM (5 μg/ml). In untreated or cells stimulated with FGF2 or IIIa–TM alone, FGFR2 co-localized with late endosomes, marked by Lamp2 expression (open arrows in **B**–**E**). Combined FGF2 and IIIa–TM treatment, however, appeared to trap much of the transfected FGFR2 at the cell membrane and reduce its co-localization with endosomal compartment (closed arrows in **F** and **G**). Results are representative of three separate experiments. Scale bars, 10 μm. (**H**) Quantification of FGFR2/Lamp2 co-localization coefficient (see the Materials and methods section) shows a significant reduction in transfected cells treated with IIIa–TM when compared with its absence. Values are means $\pm$ S.E.M., $n \geqslant 15$ from two independent experiments. *$P < 0.05$ and ***$P <$ 0.0001.

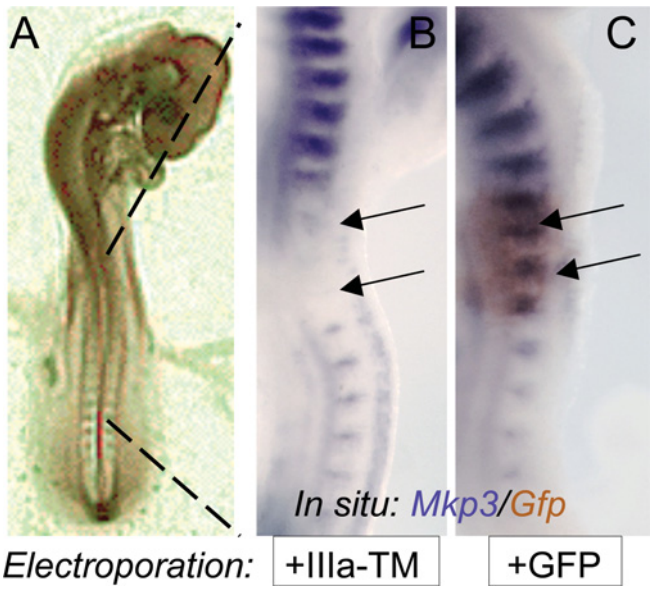

Figure 6 IIIa–TM attenuates FGFR signalling *in vivo*

(**A**) Photomicrograph of a chick embryo highlighting the region that was electroporated at stage 17 of chick embryonic development. (**B** and **C**) A clear down-regulation of *MKP3* gene expression (purple stain) was observed following electroporation of embryos with IIIa–TM (**B**), but not GFP-encoding control plasmids (**C**). The brown stain in (**C**) is *in situ* hybridization stain for GFP to show the comparable domain of GFP transduction.

detected in two other *in vivo* settings involving perturbed FGFR2 signalling. These are: (i) in FgfR2-IIIb-null mice, which lack both copies of exon 8 (IIIb) and are deficient in epithelial FGFR2 signalling [34]; and (ii) in some Pfeiffer syndrome patients who carry a mutation close to the splice acceptor site of FGFR2 exon 9 (IIIc), the mesenchymal isoform, and manifest cranial and limb phenotypes [35]. The NMD pathway is not totally efficient [31] and it is possible that, in the above scenarios, IIIa–TM is overexpressed above a threshold that NMD components, such as the Upf1 enzyme, can deal with. Indeed, loss of Upf1 leads to persistence of PTC-containing transcripts [33]. However, the observed up-regulation of IIIa–TM following perturbed FGFR2 signalling in multiple settings and tissue compartments suggests that FGFR2 signalling itself somehow has an impact on the activity of the NMD machinery to result in the stabilization of IIIa–TM and possibly other PTC-containing transcripts.

Bioavailability of ligands is a key regulator of paracrine cell signalling levels and can be controlled through sequestration of ligands by soluble proteins. For example, the levels of EGF (epidermal growth factor) and Wnt signalling are controlled in part by the naturally occurring extracellular proteins Argos [36] and Frizzled-related proteins [37] respectively. Experimental overexpression of soluble FGFR2-IIIb in mice yields phenotypes that are reminiscent of loss of FGFR2-IIIb or FGF10 genes themselves [1,34,38]. Indeed, soluble receptors are more potent than dominant-negative membrane-anchored receptors in attenuating FGF signalling [38]. Therefore IIIa–TM may attenuate FGFR signalling by sequestering FGF ligands away from membrane-anchored FGFRs and/or by forming non-functional heterotrimers with FGFRs and FGF ligands. Furthermore, the latter may interfere with normal trafficking of FGFRs, as suggested by our immunolabelling studies in Figure 5.

The inhibitory effects of IIIa–TM may depend on its glycosylation and interaction with FGF ligands. IIIa–TM carries eight putative glycoyslation sites and our present findings suggest that these are glycosylated in multiple orders *in vitro* (Figure 2C) and *in vivo* (Figures 1C and 2D). Delineating the exact type and pattern of glycosylation of these species may shed more light on its functions, since glycosylation of distinct residues on FGFRs can differentially promote or reduce their association with FGF ligands [39,40].

Our present BIAcore results show that, through an association with FGF1, soluble IIIa–TM forms a heterotrimeric complex with both IIIb and IIIc isoforms of FGFR2. We used FGF1, a pan-FGFR-activating ligand, in these assays, but it would be informative to determine whether IIIa–TM preferentially associates with distinct FGF ligands as seen in truncated soluble FGFR1 molecules [17]. Our present results indicate that IIIa–TM can interact with IIIc-activating ligands and possibly even interferes with other FGFR subtypes. Notably, IIIa–TM attenuates FGFR signalling in HEK-293T cells in the presence of FGF2, in a system where FGF4 and FGF9 are the only other endogenously produced FGFs (L.M. Wheldon and M.K. Hajihosseini, unpublished work). Furthermore, IIIa–TM attenuates FGF signalling in developing chick somites, which is dependent on FGF8 to FGFR1 signalling [26].

Relevance to AS and cancer

AS is caused by dominant-acting FGFR2 molecules that operate entirely in a ligand-dependant manner [6]. AS is hallmarked by the fusion of craniofacial sutures and by limb abnormalities accompanied by other sporadic visceral and neural defects [41]. Individuals harbouring the same mutation can present different levels of phenotypic severity. Although the ethnological origin of patients is likely to influence the severity of their defects, it is also conceivable that other modulatory molecules such as IIIa–TM could contribute to specific defects. Two specific examples include cleft palate [42] and blind colon [41], phenotypes that are reminiscent of complete loss of FGF10 or FGFR2-IIIb signalling in mice [1,43].

How can IIIa–TM induce loss-of-FGFR2 function when AS-type mutations are thought to act in a gain-of-function manner? Normally, epithelial and mesenchymal cells engage in a cross-talk through mutually exclusive expression of FGFR2-IIIb and FGFR2-IIIc isoforms and their respective activating ligands (see the Introduction, and Supplementary Figure S3 at http://www.BiochemJ.org/bj/436/bj4360071add.htm). It has been shown that AS-mutant receptors act predominantly in the mesenchyme through an illegitimate interaction with FgfR2-IIIb-activating ligands, such as FGF10 [44]. Thus membrane-anchored AS-mutant receptors and up-regulated IIIa–TM combined could compete with epithelially expressed FGFR2-IIIb for its cognate ligand FGF10 to cause a loss of FGFR2-IIIb function in epithelial cells. In support of this hypothesis, we have found that reducing the bioavailability of FGF10 in FgfR2-IIIc$^{+/\Delta}$ mice (i.e. in FgfR2-IIIc$^{+/\Delta}$ and Fgf10$^{+/-}$-double mutants) accentuates this competition and results in the occurrence of blind colon and cleft palate in a significant number of double mutants (Supplementary Figure S3; and [23])

IIIa–TM may not be the only soluble receptor to become overexpressed in AS patients [45]. Nonetheless, a detailed survey of these patients for IIIa–TM expression, together with experimental up-regulation of IIIa–TM in a spatially and temporally controlled manner in wild-type and mutant mouse models, would help delineate the roles we have postulated in the present study.

Soluble FGFRs have been also been isolated from a variety of tumour cells [46–49]. Interestingly, a Pfeiffer-syndrome-type FGFR2 mutation that causes IIIa–TM up-regulation (described above) [35] is also the cause of colorectal cancer [50]. It is not clear whether expression of soluble receptors such as IIIa–TM are the cause or the consequence of cancer, but our characterizations suggest that IIIa–TM is likely to act as an inhibitor of FGFR signalling in the context of tumorigenesis. It is interesting to note then that loss-of-FGFR2 function has been associated with specific types of astrocytomas and bladder cancers [51,52].

AUTHOR CONTRIBUTION

Lee Wheldon biochemically characterized the IIIa–TM protein, conducted the BIAcore, signalling and trafficking assays, and contributed to the writing of the paper; Naila Khodabukus cloned IIIa–TM; Susannah Patey helped with the BIAcore assays; Terence Smith performed the electroporations; John Heath contributed to the writing of the manuscript; Mohammad Hajihosseini conceived the study idea, conducted the mouse breeding, supervised the cloning of IIIa–TM, and wrote the bulk of the paper.

ACKNOWLEDGEMENTS

We are very grateful to Dr Charles Brearley, Dr Saverio Brogna and Professor David Richardson for critical reading of the manuscript prior to submission, and apologize to colleagues whose work could not be cited due to space limitations.

FUNDING

This work was supported, in part, by the CRUK [grant number CA3094 (to J.K.H.)], and The Royal Society (to M.K.H.)

REFERENCES

1 Sekine, K., Ohuchi, H., Fujiwara, M., Yamasaki, M., Yoshizawa, T., Sato, T., Yagishita, N., Matsui, D., Koga, Y., Itoh, N. and Kato, S. (1999) Fgf10 is essential for limb and lung formation. Nat. Genet. **21**, 138–141
2 Saito, T. and Fukumoto, S. (2009) Fibroblast growth factor 23 (FGF23) and disorders of phosphate metabolism. Int. J. Pediatr. Endocrinol. **2009**, 496514
3 Meyers, E. N., Lewandoski, M. and Martin, G. R. (1998) An Fgf8 mutant allelic series generated by Cre- and Flp-mediated recombination. Nat. Genet. **18**, 136–141
4 Naski, M. C., Wang, Q., Xu, J. and Ornitz, D. M. (1996) Graded activation of fibroblast growth factor receptor 3 by mutations causing achondroplasia and thanatophoric dysplasia. Nat. Genet. **13**, 233–237
5 Hajihosseini, M. K. (2008) Fibroblast growth factor signalling in cranial suture development and pathogenesis. Front. Oral Biol. **12**, 160–177
6 Wilkie, A. O. (2005) Bad bones, absent smell, selfish testes: the pleiotropic consequences of human FGF receptor mutations. Cytokine Growth Factor Rev. **16**, 187–203
7 McKeehan, W. L., Wang, F. and Kan, M. (1998) The heparan sulfate-fibroblast growth factor family: diversity of structure and function. Prog. Nucleic Acid Res. Mol. Biol. **59**, 135–176
8 Beenken, A. and Mohammadi, M. (2009) The FGF family: biology, pathophysiology and therapy. Nat. Rev. Drug Discov. **8**, 235–253
9 Hajihosseini, M. K., Lalioti, M. D., Arthaud, S., Burgar, H. R., Brown, J. M., Twigg, S. R., Wilkie, A. O. and Heath, J. K. (2004) Skeletal development is regulated by fibroblast growth factor receptor 1 signalling dynamics. Development **131**, 325–335
10 Tsang, M. and Dawid, I. B. (2004) Promotion and attenuation of FGF signalling through the Ras-MAPK pathway. Sci. STKE **2004**, pe17
11 Wheldon, L. M., Haines, B. P., Rajappa, R., Mason, I., Rigby, P. W. and Heath, J. K. (2010) Critical role of FLRT1 phosphorylation in the interdependent regulation of FLRT1 function and FGF receptor signalling. PLoS ONE **5**, e10264
12 Kuro-o, M. (2010) Klotho. Pflugers Arch. **459**, 333–343
13 Werner, S., Duan, D. S., de Vries, C., Peters, K. G., Johnson, D. E. and Williams, L. T. (1992) Differential splicing in the extracellular region of fibroblast growth factor receptor 1 generates receptor variants with different ligand-binding specificities. Mol. Cell. Biol. **12**, 82–88
14 Burgar, H. R., Burns, H. D., Elsden, J. L., Lalioti, M. D. and Heath, J. K. (2002) Association of the signalling adaptor FRS2 with fibroblast growth factor receptor 1 (Fgfr1) is mediated by alternative splicing of the juxtamembrane domain. J. Biol. Chem. **277**, 4018–4023
15 Peters, K. G., Werner, S., Chen, G. and Williams, L. T. (1992) Two FGF receptor genes are differentially expressed in epithelial and mesenchymal tissues during limb formation and organogenesis in the mouse. Development **114**, 233–243
16 Zhang, X., Ibrahimi, O. A., Olsen, S. K., Umemori, H., Mohammadi, M. and Ornitz, D. M. (2006) Receptor specificity of the fibroblast growth factor family. The complete mammalian FGF family. J. Biol. Chem. **281**, 15694–15700
17 Duan, D. S., Werner, S. and Williams, L. T. (1992) A naturally occurring secreted form of fibroblast growth factor (FGF) receptor 1 binds basic FGF in preference over acidic FGF. J. Biol. Chem. **267**, 16076–16080
18 Hanneken, A. (2001) Structural characterization of the circulating soluble FGF receptors reveals multiple isoforms generated by secretion and ectodomain shedding. FEBS Lett. **489**, 176–181
19 Maquat, L. E. (2005) Nonsense-mediated mRNA decay in mammals. J. Cell Sci. **118**, 1773–1776
20 Hajihosseini, M. K., Wilson, S., De Moerlooze, L. and Dickson, C. (2001) A splicing switch and gain-of-function mutation in FgfR2-IIIc hemizygotes causes Apert/Pfeiffer-syndrome-like phenotypes. Proc. Natl. Acad. Sci. U.S.A. **98**, 3855–3860
21 Oldridge, M., Zackai, E. H., McDonald-McGinn, D. M., Iseki, S., Morriss-Kay, G. M., Twigg, S. R., Johnson, D., Wall, S. A., Jiang, W., Theda, C. et al. (1999) *De novo* alu-element insertions in FGFR2 identify a distinct pathological basis for Apert syndrome. Am. J. Hum. Genet. **64**, 446–461
22 Bochukova, E. G., Roscioli, T., Hedges, D. J., Taylor, I. B., Johnson, D., David, D. J., Deininger, P. L. and Wilkie, A. O. (2009) Rare mutations of FGFR2 causing Apert syndrome: identification of the first partial gene deletion, and an Alu element insertion from a new subfamily. Hum. Mutat. **30**, 204–211
23 Hajihosseini, M. K., Duarte, R., Pegrum, J., Donjacour, A., Lana-Elola, E., Rice, D. P., Sharpe, J. and Dickson, C. (2009) Evidence that Fgf10 contributes to the skeletal and visceral defects of an Apert syndrome mouse model. Dev. Dyn. **238**, 376–385
24 Hajihosseini, M. K. and Dickson, C. (1999) A subset of fibroblast growth factors (Fgfs) promote survival, but Fgf-8b specifically promotes astroglial differentiation of rat cortical precursor cells. Mol. Cell. Neurosci. **14**, 468–485
25 Anderson, J., Burns, H. D., Enriquez-Harris, P., Wilkie, A. O. and Heath, J. K. (1998) Apert syndrome mutations in fibroblast growth factor receptor 2 exhibit increased affinity for FGF ligand. Hum. Mol. Genet. **7**, 1475–1483
26 Smith, T. G., Sweetman, D., Patterson, M., Keyse, S. M. and Munsterberg, A. (2005) Feedback interactions between MKP3 and ERK MAP kinase control scleraxis expression and the specification of rib progenitors in the developing chick somite. Development **132**, 1305–1314
27 Terada, M., Shimizu, A., Sato, N., Miyakaze, S. I., Katayama, H. and Kurokawa-Seo, M. (2001) Fibroblast growth factor receptor 3 lacking the Ig IIIb and transmembrane domains secreted from human squamous cell carcinoma DJM-1 binds to FGFs. Mol. Cell. Biol. Res. Commun. **4**, 365–373
28 Nelson, R. W., Nedelkov, D. and Tubbs, K. A. (2000) Biosensor chip mass spectrometry: a chip-based proteomics approach. Electrophoresis **21**, 1155–1163
29 Miki, T., Bottaro, D. P., Fleming, T. P., Smith, C. L., Burgess, W. H., Chan, A. M. and Aaronson, S. A. (1992) Determination of ligand-binding specificity by alternative splicing: two distinct growth factor receptors encoded by a single gene. Proc. Natl. Acad. Sci. U.S.A. **89**, 246–250
30 Jones, R. B., Wang, F., Luo, Y., Yu, C., Jin, C., Suzuki, T., Kan, M. and McKeehan, W. L. (2001) The nonsense-mediated decay pathway and mutually exclusive expression of alternatively spliced FGFR2IIIb and -IIIc mRNAs. J. Biol. Chem. **276**, 4158–4167
31 Muhlemann, O., Eberle, A. B., Stalder, L. and Zamudio Orozco, R. (2008) Recognition and elimination of nonsense mRNA. Biochim. Biophys. Acta **1779**, 538–549
32 Lewis, B. P., Green, R. E. and Brenner, S. E. (2003) Evidence for the widespread coupling of alternative splicing and nonsense-mediated mRNA decay in humans. Proc. Natl. Acad. Sci. U.S.A. **100**, 189–192
33 Mendell, J. T., Sharifi, N. A., Meyers, J. L., Martinez-Murillo, F. and Dietz, H. C. (2004) Nonsense surveillance regulates expression of diverse classes of mammalian transcripts and mutes genomic noise. Nat. Genet. **36**, 1073–1078
34 De Moerlooze, L., Spencer-Dene, B., Revest, J., Hajihosseini, M., Rosewell, I. and Dickson, C. (2000) An important role for the IIIb isoform of fibroblast growth factor receptor 2 (FGFR2) in mesenchymal-epithelial signalling during mouse organogenesis. Development **127**, 483–492

35 Tsukuno, M., Suzuki, H. and Eto, Y. (1999) Pfeiffer syndrome caused by haploinsufficient mutation of FGFR2. J. Craniofac. Genet. Dev. Biol. **19**, 183–188
36 Klein, D. E., Nappi, V. M., Reeves, G. T., Shvartsman, S. Y. and Lemmon, M. A. (2004) Argos inhibits epidermal growth factor receptor signalling by ligand sequestration. Nature **430**, 1040–1044
37 Kawano, Y. and Kypta, R. (2003) Secreted antagonists of the Wnt signalling pathway. J. Cell Sci. **116**, 2627–2634
38 Celli, G., LaRochelle, W. J., Mackem, S., Sharp, R. and Merlino, G. (1998) Soluble dominant-negative receptor uncovers essential roles for fibroblast growth factors in multi-organ induction and patterning. EMBO J. **17**, 1642–1655
39 Duchesne, L., Tissot, B., Rudd, T. R., Dell, A. and Fernig, D. G. (2006) N-glycosylation of fibroblast growth factor receptor 1 regulates ligand and heparan sulfate co-receptor binding. J. Biol. Chem. **281**, 27178–27189
40 Polanska, U. M., Duchesne, L., Harries, J. C., Fernig, D. G. and Kinnunen, T. K. (2009) N-Glycosylation regulates fibroblast growth factor receptor/EGL-15 activity in *Caenorhabditis elegans in vivo*. J. Biol. Chem. **284**, 33030–33039
41 Cohen, Jr, M. M. and Kreiborg, S. (1993) An updated pediatric perspective on the Apert syndrome. Am. J. Dis. Child. **147**, 989–993
42 Slaney, S. F., Oldridge, M., Hurst, J. A., Moriss-Kay, G. M., Hall, C. M., Poole, M. D. and Wilkie, A. O. (1996) Differential effects of FGFR2 mutations on syndactyly and cleft palate in Apert syndrome. Am. J. Hum. Genet. **58**, 923–932
43 Fairbanks, T. J., De Langhe, S., Sala, F. G., Warburton, D., Anderson, K. D., Bellusci, S. and Burns, R. C. (2004) Fibroblast growth factor 10 (Fgf10) invalidation results in anorectal malformation in mice. J. Pediatr. Surg. **39**, 360–365
44 Ibrahimi, O. A., Zhang, F., Eliseenkova, A. V., Itoh, N., Linhardt, R. J. and Mohammadi, M. (2004) Biochemical analysis of pathogenic ligand-dependent FGFR2 mutations suggests distinct pathophysiological mechanisms for craniofacial and limb abnormalities. Hum. Mol. Genet. **13**, 2313–2324
45 Tanimoto, Y., Yokozeki, M., Hiura, K., Matsumoto, K., Nakanishi, H., Matsumoto, T., Marie, P. J. and Moriyama, K. (2004) A soluble form of fibroblast growth factor receptor 2 (FGFR2) with S252W mutation acts as an efficient inhibitor for the enhanced osteoblastic differentiation caused by FGFR2 activation in Apert syndrome. J. Biol. Chem. **279**, 45926–45934
46 Jang, J. H., Shin, K. H., Park, Y. J., Lee, R. J., McKeehan, W. L. and Park, J. G. (2000) Novel transcripts of fibroblast growth factor receptor 3 reveal aberrant splicing and activation of cryptic splice sequences in colorectal cancer. Cancer Res. **60**, 4049–4052
47 Takaishi, S., Sawada, M., Morita, Y., Seno, H., Fukuzawa, H. and Chiba, T. (2000) Identification of a novel alternative splicing of human FGF receptor 4: soluble-form splice variant expressed in human gastrointestinal epithelial cells. Biochem. Biophys. Res. Commun. **267**, 658–662
48 Ezzat, S., Zheng, L., Yu, S. and Asa, S. L. (2001) A soluble dominant negative fibroblast growth factor receptor 4 isoform in human MCF-7 breast cancer cells. Biochem. Biophys. Res. Commun. **287**, 60–65
49 Jang, J. H. (2002) Identification and characterization of soluble isoform of fibroblast growth factor receptor 3 in human SaOS-2 osteosarcoma cells. Biochem. Biophys. Res. Commun. **292**, 378–382
50 Jang, J. H., Shin, K. H. and Park, J. G. (2001) Mutations in fibroblast growth factor receptor 2 and fibroblast growth factor receptor 3 genes associated with human gastric and colorectal cancers. Cancer Res. **61**, 3541–3543
51 Ricol, D., Cappellen, D., El Marjou, A., Gil-Diez-de-Medina, S., Girault, J. M., Yoshida, T., Ferry, G., Tucker, G., Poupon, M. F., Chopin, D. et al. (1999) Tumour suppressive properties of fibroblast growth factor receptor 2-IIIb in human bladder cancer. Oncogene **18**, 7234–7243
52 Yamaguchi, F., Saya, H., Bruner, J. M. and Morrison, R. S. (1994) Differential expression of two fibroblast growth factor-receptor genes is associated with malignant progression in human astrocytomas. Proc. Natl. Acad. Sci. U.S.A. **91**, 484–488

Received 18 June 2010/17 February 2011; accepted 28 February 2011
Published as BJ Immediate Publication 28 February 2011, doi:10.1042/BJ20100884

Biochem. J. (2011) **436**, 71–81 (Printed in Great Britain) doi:10.1042/BJ20100884

online data

SUPPLEMENTARY ONLINE DATA

Identification and characterization of an inhibitory fibroblast growth factor receptor 2 (FGFR2) molecule, up-regulated in an Apert Syndrome mouse model

Lee M. WHELDON*[1], Naila KHODABUKUS*, Susannah J. PATEY*, Terence G. SMITH†, John K. HEATH* and Mohammad K. HAJIHOSSEINI†[2]

*School of Biosciences, University of Birmingham, Edgbaston B15 2TT, U.K., and †School of Biological Sciences, University of East Anglia, Norwich, Norfolk NR4 7TJ, U.K.

agtttagttgaggataccactttagaaccagaagagccaccaaccaaataccaaa
tctcccaaccagaagcgtacgtggttgccccgggggaatcgctagagttgcagtg
catgttgaaagatgccgccgtgatcagttggactaaggatggggtgcacttgggg
cccaacaataggacagtgcttattggggagtatctccagataaaaggtgccacac
ctagagactccggcctctatgcttgtactgcagctaggacggtagacagtgaaac
ttggtacttcatggtgaatgtcacagatgccatctcatctggagatgacgaggac
gacacagatagctccgaagacgttgtcagtgagaacaggagcaaccagagagcac
cgtactggaccaacaccgagaagatggagaagcggctccacgctgtccctgccgc
caacactgtgaagttccgctgtccggctgggggggaatccaacgcccacaatgagg
tggttaaaaaacgggaaggagtttaagcaggagcatcgcattggaggctataagg
tacgaaaccagcactggagccttattatggaaagtgtggtcccgtcagacaaagg
caactacacctgcctggtggagaatgaatacgggtccatcaaccacacctaccac
ctcgatgtcgttgaacggtcaccacaccgtcccatcctccaagctggactgcctg
caaatgcctccacggtggtcggaggggatgtggagtttgtctgcaaggtttacag
cgatgcccagccccacatccagtggatcaagcacgtggaaaagaacggcagtaaa
tacgggcctgatgggctgccctacctcaaggtcctgaagcgcctgtga

Colour coding:
Green = FGFR2 exon 2 /exon 3 junction.
Bold = Cysteine residues that pair to form the Ig-like domains (see Figure 1).
Underlined = The so called 'Acid box' region
Red = Predicted potential N-glycosylation sites/residues (NetNglyc 1.0)
Orange = First nine bases of exon 10 (TM)
Bold orange = STOP codon

Figure S1 Nucleotide sequence of 873 bp 'full-length' IIIa–TM amplified by RT–PCR using primers P3 and P4

Colour coding is indicated on the Figure.

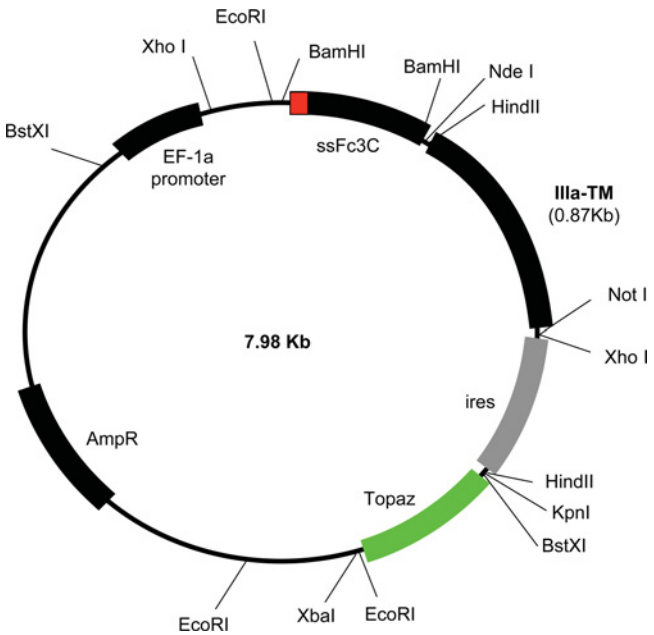

Figure S2 Schematic representation of the ires-Topaz-PEF-BOS plasmid into which the ss-3C-FC-IIIa–TM fragments were cloned as an NdeI/NotI 0.87 kb fragment

[1] Present address: Molecular Biology and Immunology Group, Centre for Biomolecular Sciences, University of Nottingham, Nottingham NG7 2RD, U.K.
[2] To whom correspondence should be addressed (email m.k.h@uea.ac.uk).

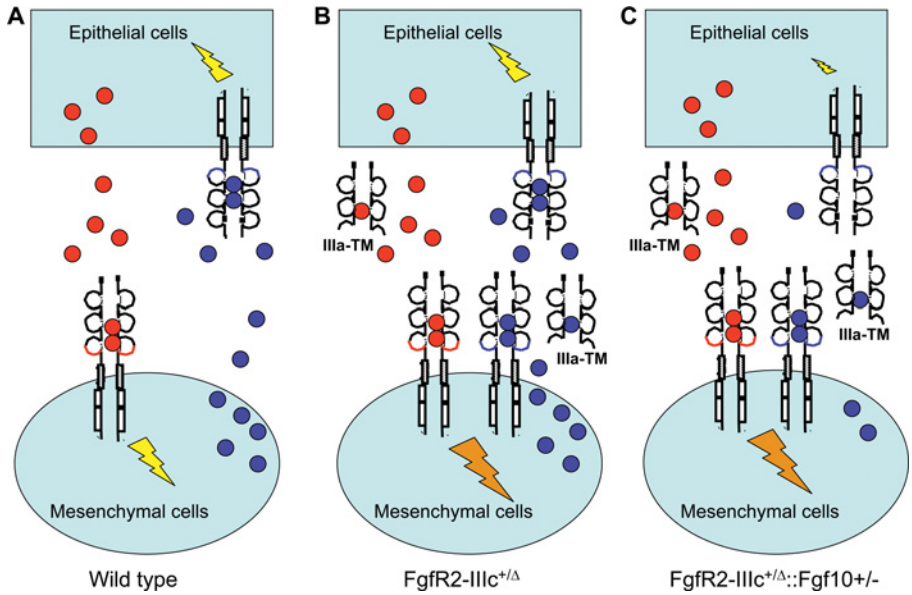

Figure S3 A hypothetical scenario by which IIIa–TM induces loss-of-FGFR2 function

IIIa–TM competes with membrane-bound receptors for FGF ligand(s) following its up-regulation in FgfR2-IIIc$^{+/\Delta}$ mice. In (**C**), a heterozygous reduction in FGF10 may accentuate this competition and result in loss-of-FGF10-to-FGFR2-IIIb signalling in epithelial cells. Yellow, normal level of FGFR2 signalling in either epithelial or mesenchymal cells in wild-type tissues; red circles, FGFR2-IIIc-activating ligands produced by epithelial cells; navy blue circles, FGFR2-IIIb-activating ligands produced by mesenchymal cells; red and blue Ig-III-like domains, FGFR2-IIIc and FGFR2-IIIb respectively; orange, elevated levels of FGFR2 signalling in mesenchymal cells of FgfR2-IIIc$^{+/\Delta}$ mice, as a result of FGFR2-IIIb up-regulation and autocrine signalling. Truncated receptors, IIIa–TM.

Received 18 June 2010/17 February 2011; accepted 28 February 2011
Published as BJ Immediate Publication 28 February 2011, doi:10.1042/BJ20100884